Amine-Rich Polyelectrolyte Multilayer Nanoreactors for in Situ Gold Nanoparticle Synthesis

Khek-Khiang Chia,[†] Robert E. Cohen,*[,†,‡] and Michael F. Rubner*[,‡,§]

Department of Chemical Engineering, Center for Materials Science and Engineering, and Department of Materials Science and Engineering, Massachusetts Institute of Technology, Cambridge, Massachusetts 02139

Received August 8, 2008. Revised Manuscript Received September 12, 2008

In situ synthesis of inorganic clusters in polyelectrolyte multilayers (PEMs) has typically relied on free carboxylic acid groups as the binding sites, limiting the scheme to the loading of cationic precursor reagents. The use of amine groups for similar purposes has not been demonstrated because of the challenge of incorporating free amine groups that are not paired with the oppositely charged groups residing on the polyanion of the PEM. In this paper, we use specific PEM assembly conditions to produce ultrathin conformal films of PAH/PAA (poly(allylamine hydrochloride)/poly(acrylic acid)) and PAH/PSS (poly(styrene sulfonate)) that upon suitable postassembly treatment undergo substantial molecular rearrangements that generate free amine groups in the films. These PEMs are capable of binding anionic precursors including complexes widely used for the synthesis of gold nanoparticles. On the basis of our understanding of the gold binding mechanisms, we demonstrate systematic control over the size and spatial distribution of gold nanoparticles in the films by changing the PEM assembly and postassembly treatment conditions.

Introduction

Much of the interest in the layer-by-layer assembly of polyelectrolyte multilayers (PEMs) arises from the ease by which the molecular architecture of the resultant thin film can be controlled through adjustments of assembly and postassembly treatment conditions.[1−11] The precise control over the molecular architecture of the PEMs facilitates the incorporation of inorganic nanoparticles into the films, which have a broad range of potential applications due to the optical,[12−14] catalytic,[15,16] and magnetic[17] properties that arise from the nanoparticles' large surface-area-to-volume ratios and quantum confinement effects.[18−20]

PEM/nanoparticle composites have been synthesized via the layer-by-layer assembly of prefabricated inorganic nanoparticles or polyelectrolyte-stabilized metal ion complexes with an oppositely charged polyelectrolyte.[21−26] The assembly of PEM/gold nanoparticle composites,[12,14,22,27−29] in particular, has been demonstrated and may provide a route to potential biological applications due to the nontoxicity, biocompatibility, ease of imaging and versatility of surface chemistry of gold nanoparticles. The use of PEMs as nanoreactors offers the promise for precise control over the

* Corresponding author. E-mail: recohen@mit.edu (R.E.C.); rubner@mit.edu (M.F.R.).
[†] Department of Chemical Engineering, Massachusetts Institute of Technology.
[‡] Center for Materials Science and Engineering, Massachusetts Institute of Technology.
[§] Department of Materials Science and Engineering, Massachusetts Institute of Technology.

(1) Mendelsohn, J. D.; Barrett, C. J.; Chan, V. V.; Pal, A. J.; Mayes, A. M.; Rubner, M. F. *Langmuir* **2000**, *16*, 5017–5023.
(2) Wang, T. C.; Rubner, M. F.; Cohen, R. E. *Langmuir* **2002**, *18*, 3370–3375.
(3) Hiller, J.; Mendelsohn, J. D.; Rubner, M. F. *Nat. Mater.* **2002**, *1*, 59–63.
(4) Cho, J.; Caruso, F. *Macromolecules* **2003**, *36*, 2845–2851.
(5) Ono, S. S.; Decher, G. *Nano Lett.* **2006**, *6*, 592–598.
(6) Peez, R. F.; Dermody, D. L.; Franchina, J. G.; Jones, S. J.; Bruening, M. L.; Bergbreiter, D. E.; Crooks, R. M. *Langmuir* **1998**, *14*, 4232–4237.
(7) Srivastava, S.; Ball, V.; Podsiadlo, P.; Lee, J.; Ho, P.; Kotov, N. A. *J. Am. Chem. Soc.* **2008**, *130*, 3748–3749.
(8) Sui, Z.; Schlenoff, J. B. *Langmuir* **2004**, *20*, 6026–6031.
(9) Shutava, T.; Prouty, M.; Kommireddy, D.; Lvov, Y. *Macromolecules* **2005**, *38*, 2850–2858.
(10) Dejugnat, C.; Sukhorukov, G. B. *Langmuir* **2004**, *20*, 7265–7269.
(11) Sukhishvili, S. A. *Curr. Opin. Colloid Interface Sci.* **2005**, *10*, 37–44.
(12) Malikova, N.; Pastoriza-Santos, I.; Schierhorn, M.; Kotov, N. A.; Liz-Marzán, L. M. *Langmuir* **2002**, *18*, 3694–3697.
(13) Schneider, G.; Decher, G.; Nerambourg, N.; Praho, R.; Werts, M. H. V.; Blanchard-Desce, M. *Nano Lett.* **2006**, *6*, 530–536.
(14) Schrof, W.; Rozouvan, S.; Keuren, E. V.; Horn, D.; Schmitt, J.; Decher, G. *Adv. Mater.* **1998**, *10*, 338–341.
(15) Dotzauer, D. M.; Dai, J.; Sun, L.; Bruening, M. L. *Nano Lett.* **2006**, *6*, 2268–2272.
(16) Dai, J.; Bruening, M. L. *Nano Lett.* **2002**, *2*, 497–501.
(17) Sun, S.; ers, S.; Thomson, T.; Baglin, J. E. E.; Toney, M. F.; Hamann, H. F.; Murray, C. B.; Terris, B. D. *J. Phys. Chem. B* **2003**, *107*, 5419–5425.
(18) Henglein, A. *Chem. Rev.* **1989**, *89*, 1861.
(19) Brus, L. *Appl. Phys. A: Mater. Sci. Process.* **1991**, 53.
(20) Alivisatos, A. P. *Science* **1996**, *271*, 933–937.
(21) Caruso, F.; Lichtenfeld, H.; Giersig, M.; Möhwald, H. *J. Am. Chem. Soc.* **1998**, *120*, 8523–8524.
(22) Dong, W. F.; Sukhorukov, G. B.; Möhwald, H. *Phys. Chem. Chem. Phys.* **2003**, *5*, 3003–3012.
(23) Schmitt, J.; Decher, G.; Dressick, W. J.; Brandow, S. L.; Geer, R. E.; Shashidhar, R.; Calvert, J. M. *Adv. Mater.* **1997**, *9*, 61–65.
(24) Wang, Y.; Tang, Z. Y.; Correa-Duarte, M. A.; Liz-Marzán, L. M.; Kotov, N. A. *J. Am. Chem. Soc.* **2003**, *125*, 2830–2831.
(25) Kidambi, S.; Dai, J. H.; Li, J.; Bruening, M. L. *J. Am. Chem. Soc.* **2004**, *126*, 2658–2659.
(26) Kommireddy, D. S.; Patel, A. A.; Shutava, T. G.; Mills, D. K.; Lvov, Y. M. *J. Nanosci. Nanotechnol.* **2005**, *5*, 1081–1087.
(27) Cho, J. H.; Caruso, F. *Chem. Mater.* **2005**, *17*, 4547–4553.
(28) Salata, O. V. *J. Nanobiotechnol.* **2004**, *2*, 3.
(29) Jiang, G. Q.; Baba, A.; Ikarashi, H.; Xu, R. S.; Locklin, J.; Kashif, K. R.; Shinbo, K.; Kato, K.; Kaneko, F.; Advincula, R. *J. Phys. Chem. C* **2007**, *111*, 18687–18694.

10.1021/cm802166s CCC: $40.75
Published on Web 10/17/2008

in situ growth of inorganic nanoparticles in preformed, conformal PEM coatings on a variety of substrate materials of essentially any size and shape.[2] In this approach, the PEMs are typically assembled to contain free functional groups that can bind inorganic ion precursors. One of the common methods involves the incorporation of free carboxylic acid groups that serve as binding sites for cationic precursors, which are then reduced to inorganic nanoparticles.[2,30−32] However, the use of free carboxylic acid groups is limited to the binding of cationic precursors (e.g., Ag^+) and therefore cannot be used to bind anionic precursors such as gold complex ions (e.g., $AuCl_4^-$).

Polymers containing amine groups have been widely used as the source of binding sites for anionic gold complex ions and as capping agents limiting nanoparticle growth and agglomeration.[27,33−35] However, for the case of PEMs, the application of these amine-gold chemistries in the in situ synthesis of gold nanoparticles has not been demonstrated. The challenge in doing so lies in the fact that under typical assembly conditions, most amine groups in PEMs are ionized and paired with oppositely charged groups residing on the polyanion that is used in the PEM assembly, for example poly(acrylic acid) (PAA) or poly(styrene sulfonate) (PSS), which prevents their binding to other ions. The successful incorporation of free amine groups in PEMs is complicated by the fact that the high assembly pH required to produce free amine groups often renders commonly used polycations, such as poly(allylamine hydrochloride) (PAH), insoluble. In this paper, we overcome these challenges by generating free amine groups using specific postassembly processing conditions that introduce molecular rearrangements that produce the free amine groups needed for nanoparticle synthesis. These molecular rearrangements only occur in PEMs assembled under very specific conditions, such as (PAH7.5/PAA3.5) and (PAH9.3/PSS9.3), where the numbers represent the polyelectrolyte solution pH during layer-by-layer assembly. We demonstrate that an understanding of these postassembly transitions can be used to control the in situ synthesis of gold nanoparticles.

Experimental Section

Materials. Poly(allylamine hydrochloride) (PAH) (M_w 70 000) (Sigma-Aldrich, product no. 283223, subsequently labeled by the company as having M_w ~56 000) was used as the polycation; poly(acrylic acid) (PAA) (M_w 90 000, 25% aqueous solution) (Polysciences, catalog no. 03326-250, subsequently labeled by the company as having M_w >200 000) and poly(sodium-4-styrene sulfonate) (PSS) (M_w 70 000) (Sigma-Aldrich) were used as polyanions. All polyelectrolytes were used as received without further purification and were prepared as 1×10^{-2} M solutions (based on the repeat-unit molecular weight) in ultrapure 18 MΩ·cm deionized water (Millipore Milli-Q). The polyelectrolyte solutions were adjusted to the desired pH (±0.01) with 1 M HCl or 1 M NaOH. The substrates used for PEM assembly were glass slides (VWR International), polished single-crystal (⟨100⟩) silicon wafers (WaferNet), and tissue-culture polystyrene (PS) (Nalge Nunc International). Gold(III) chloride trihydrate ($HAuCl_4 \cdot 3H_2O$) (Sigma-Aldrich) was prepared as 5 mM solutions (pH 2.3) with Millipore water and stored away from light.

PEM Assembly and Characterization. PEMs were formed by immersing substrates into a polycation solution (PAH) for 15 min followed by three water rinsing steps (2, 1, 1 min), using a programmable slide stainer (Zeiss). The substrates were then immersed into a polyanion solution (PAA or PSS) for 15 min followed by identical rinsing steps. A single adsorption of polycation followed by polyanion on the substrate is defined as a bilayer. A PEM notation of (PolyA *x*/ PolyB *y*)$_z$ is used, where PolyA represents the first polyelectrolyte adsorbed onto the substrate; its assembly pH, *x*; the second polyelectrolyte, PolyB; its assembly pH, *y*; and the total number of bilayers, *z*. In this study, all PEMs were processed and characterized immediately after film assembly. Dry film thickness was measured using a Tencor P10 profilometer. In some cases, film thickness, in contact with a selected aqueous solution, was measured in situ using a quartz cell and a J.A.Woollam Co., Inc. VASE spectroscopic ellipsometer. In situ ellipsometry measurements were collected 10 min after the sample was immersed in the desired solution. Data were collected between 300 and 1000 nm at a 70° incidence angle and analyzed with WVASE32 software package, fitted with a Cauchy model, which assumes the real part of the refractive index, n_f, as a function of wavelength, λ, to be $n_f(\lambda) = A_n + B_n/\lambda^2 + C_n/\lambda^4$, where A_n, B_n, and C_n are constants. The refractive index of 5 mM gold salt solution was assumed to be close to that of water (1.33). The extent of swelling of the PEMs in solution was defined as

$$\text{Extent of swelling} = \frac{\text{Film thickness in solution} - \text{Film thickness in dry state}}{\text{Film thickness in dry state}} \times 100\%$$

Gold Loading and Reduction. PEMs were immersed in gold salt solutions (5 mM) at the desired pH in the dark for 15 min, followed by three water rinse steps (2, 1, 1 min), and then air-dried at room temperature. The gold salt solution was adjusted to the desired pH (±0.01) with 1 M HCl or 1 M NaOH. The gold-salt-loaded samples were then irradiated with an ultraviolet (UV) lamp (365 nm, UVL-28 EL series, UVP, 1300 $\mu W/cm^2$) for 35 h. It should be noted that at a higher UV intensity, the reduction time can be greatly reduced to an upper bound of 12 h.

Gold Nanoparticle Characterization. *UV−Vis Spectrophotometry.* Optical transmission measurements were conducted using a Varian Cary5E spectrophotometer using air as the baseline. The absorbance values are from specimens with PEMs on both sides of the glass substrates. *Transmission Electron Microscopy (TEM).* PEMs assembled on PS substrates were embedded in epoxy (Ladd Research LR white resin) and stored at ambient conditions for 24 h prior to microtoming using a RMC MT-X ultramicrotome with a diamond knife (Diatome) at room temperature. Samples microtomed at approximately 60 nm (cross-sectional thickness) were floated on a trough of DI water, collected on copper TEM grids (Structure Probe, Inc.), blotted dry, and coated with approximately 10 Å carbon using a sputter coater. TEM imaging was performed using either JEOL 200CX or JEOL 2011, operated at 200 kV. Particle size was measured for each sample using UTHSCSA ImageTool software. The TEM images are always oriented such that the PEM is sandwiched between the epoxy on the top and the substrate on the

(30) Lee, D.; Rubner, M. F.; Cohen, R. E. *Chem. Mater.* **2005**, *17*, 1099–1105.
(31) Nolte, A. J.; Rubner, M. F.; Cohen, R. E. *Langmuir* **2004**, *20*, 3304–3310.
(32) Lee, D.; Cohen, R. E.; Rubner, M. F. *Langmuir* **2005**, *21*, 9651–9659.
(33) Newman, J. D. S.; Blanchard, G. J. *J. Nanopart. Res.* **2007**, *9*, 861–868.
(34) Kim, Y.-J.; Cho, G.; Song, J. H. *J. Nanosci. Nanotechnol.* **2006**, *6*, 3373–3375.
(35) Zhu, H. G.; Pan, Z. W.; Hagaman, E. W.; Liang, C. D.; Overbury, S. H.; Dai, S. *J. Colloid Interface Sci.* **2005**, *287*, 360–365.

bottom. The reported particle sizes are the number average (μ) from at least 1000 particles. These values should be used as upper bound estimates because larger particles were more likely to be counted because of higher contrast. The standard devations (σ) for these values are also included. The particle diameters were measured by hand using software without thresholding, thereby eliminating the possibility of any software-induced bias. The particle size distribution was also generated manually on the basis of the measured particle diameters.

Results and Discussion

Role of PEM Assembly pH on Nanoparticle Growth. The assembly of PAH with various polyanions is typically carried out in the pH range of 3−8. Under these assembly conditions, the resultant PEM is comprised of fully ionized ammonium groups that are electrostatically bound to the oppositely charged polyelectrolyte.[36] To demonstrate that assembly under these conditions does not produce the concentration of free amine groups needed for gold nanoparticle synthesis, we attempted to grow nanoparticles in two representative multilayer systems: (PAH3.5/PAA3.5) and (PAH4.0/PSS4.0). (In this paper, the term "free" is used to denote the availability of the amine/ammonium groups to bind to other functional groups.) Both PEMs were immersed in gold salt solutions (5 mM $HAuCl_4$ at pH 2.3 for 15 min), rinsed with deionized (DI) water (pH ~5.5 for 2, 1, 1 min), exposed to UV light and then characterized with UV−vis spectrophotometry (see the Supporting Information). In both cases, the absence of any detectable surface plasmon resonance (SPR)[37−41] absorption bands attributable to gold nanoparticles confirmed that binding of the gold complex anions was unsuccessful. The intensity and wavelength at maximum intensity (λ_{max}) of SPR bands are known to correlate with nanoparticle size and concentration.[39,42−46]

We then examined two other multilayer systems known to undergo postassembly molecular rearrangements with low pH treatments: (PAH7.5/PAA3.5) and (PAH9.3/PSS9.3).[1,3,36,47−49] Both PEMs were immersed in gold salt solutions at different pH levels, rinsed with DI water, exposed to UV light, and characterized with UV−vis spectrophotometry. As seen in Figure 1, detectable SPR bands with λ_{max} values located between 500 and 600 nm were observed in all films

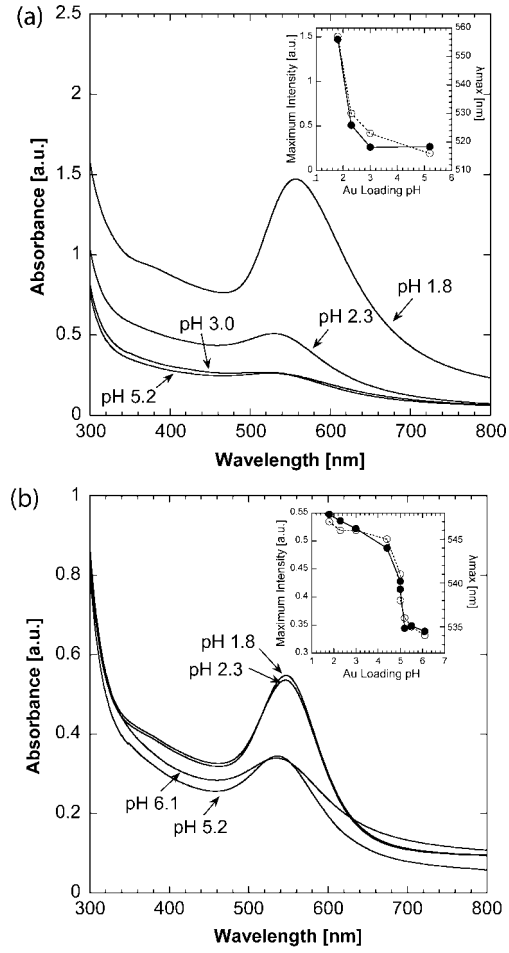

Figure 1. UV−vis absorbance spectra of (a) $(PAH7.5/PAA3.5)_{20}$ and (b) $(PAH9.3/PSS9.3)_{20}$ PEMs loaded with gold salt at pH levels between 1.8 and 6.1, rinsed with DI water and UV-reduced. Insets: Maximum intensity (closed circles) and λ_{max} (open circles) of the SPR absorbance spectra as a function of gold salt loading pH.

regardless of the solution pH used to load the gold salt. However, a dramatic increase in the peak intensities of the SPR bands was observed below a critical loading pH of ca. 2.5 for the (PAH7.5/PAA3.5) multilayer system and ca. 5.0 for the (PAH9.3/PSS9.3) multilayer system. These results indicate that some free amine groups are present in the as-assembled multilayers and that a significant increase in free amine group concentration occurs below a critical loading pH. We refer to loading at pH below and above the critical loading pHs as the high and low binding regimes, respectively.

Gold Salt Binding Mechanism. On the basis of previous studies with these particular multilayer systems,[1,3,36,47−49] we put forth the following explanations for the pH-dependent assembly and gold-salt-loading behavior of (PAH7.5/PAA3.5) and (PAH9.3/PSS9.3) thin films. Schematics of the mechanism of gold nanoparticle formation are shown in Scheme 1.

(PAH7.5/PAA3.5) Multilayer System. As assembled, the internal structure of this multilayer system is mostly comprised of fully ionized, electrostatically paired functional groups, and a small fraction of protonated free amine groups. In the low binding regime (pH >2.5), the relatively small concentration of protonated free amine groups can bind to the gold complex ions, resulting in the formation of a low concentration of gold nanoparticles after suitable UV reduc-

(36) Itano, K.; Choi, J. Y.; Rubner, M. F. *Macromolecules* **2005**, *38*, 3450–3460.
(37) Mie, G. *Ann. Phys.* **1908**, *25*, 377–445.
(38) Hayat, M. A. *Colloidal Gold: Principles, Methods and Applications*; Academic: San Diego, CA, 1991.
(39) Bohren, C. F.; Huffman, D. R. *Absorption and Scattering of Light by Small Particles*; John Wiley and Sons: New York, NY, 1983.
(40) Kreibig, U.; Vollmer, M. *Optical Properties of Metal Clusters*; Springer: Berlin, 1995.
(41) Haes, A. J.; Van Duyne, R. P. *J. Am. Chem. Soc.* **2002**, *124*, 10596–10604.
(42) Vollmer, M.; Kreibig, U. *Nuclear Physics Concepts in the Study of Atomic Cluster Physics*; Springer: Berlin, 1992.
(43) Genzel, L.; Martin, T. P. *Surf. Sci.* **1973**, *34*, 33–49.
(44) Haiss, W.; Thanh, N. T. K.; Aveyard, J.; Fernig, D. G. *Anal. Chem.* **2007**, *79*, 4215–4221.
(45) Mirkin, C. A.; Letsinger, R. L.; Mucic, R. C.; Storhoff, J. J. *Nature* **1996**, *382*, 607–609.
(46) Brust, M.; Bethell, D.; Kiely, C. J.; Schiffrin, D. J. *Langmuir* **1998**, *14*, 5425–5429.
(47) Choi, J.; Rubner, M. F. *Macromolecules* **2005**, *38*, 116–124.
(48) Hiller, J.; Rubner, M. F. *Macromolecules* **2003**, *36*, 4078–4083.
(49) Zhai, L.; Cebeci, F. C.; Cohen, R. E.; Rubner, M. F. *Nano Lett.* **2004**, *4*, 1349–1353.

Scheme 1. Gold Binding and Reduction Mechanism in (a) (PAH7.5/PAA3.5) and (b) (PAH9.3/PSS9.3) PEMs[a]

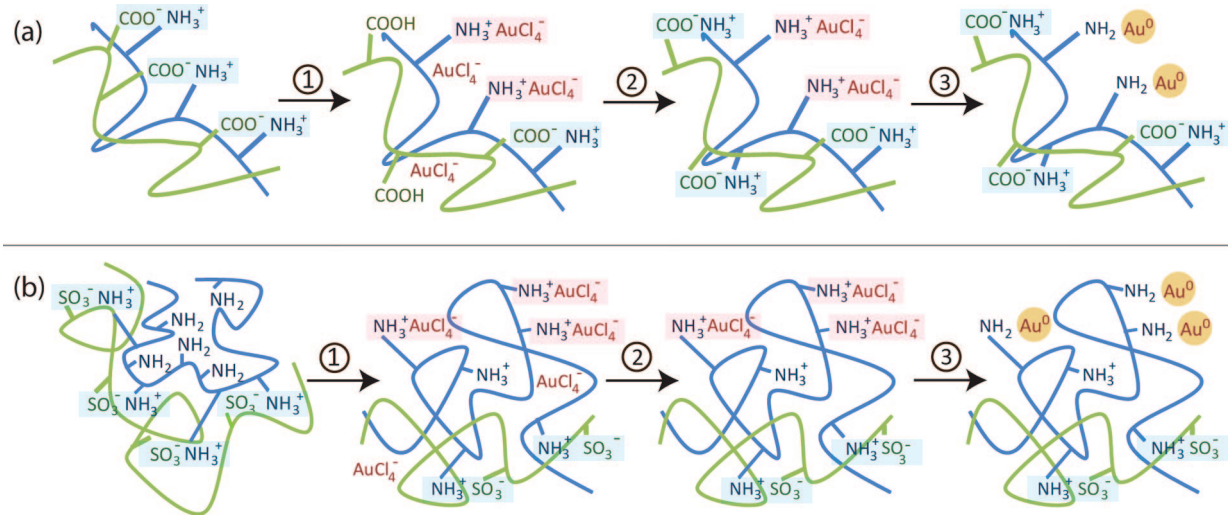

[a] (1) Gold salt loading, (2) water rinse, and (3) UV reduction. Electrostatically bound functional groups are shaded. For illustration purposes, $AuCl_4^-$ represents all negatively-charged gold complex ions, whereas the amine groups after Step 3 represent all possible functional groups with different oxidation states (e.g., imine groups).

tion (Figure 1a). In the high binding regime (pH ≤2.5), the strong acidic condition converts carboxylate groups into protonated carboxylic acid groups, thereby breaking the $COO^--NH_3^+$ electrostatic linkages formed during multilayer assembly. This process, in turn, renders the ammonium groups available for gold salt binding (Scheme 1a, Step 1). When a sufficient number of $COO^--NH_3^+$ electrostatic linkages are broken, the film undergoes a spinodal decomposition-type of molecular rearrangement that in earlier studies was shown to result in a porosity transition.[1,3,49] This process further generates free ammonium groups and increases the binding capacity of the film dramatically, as indicated from the peak intensity and λ_{max} values of the SPR bands (Figure 1a). The DI water rinse steps (pH ~5.5 for 2, 1, 1 min) removes unbound gold complex ions and deprotonates carboxylic acid groups into carboxylates which then bind to some of the ammonium groups to reform COO^- $-NH_3^+$ electrostatic linkages, thereby maintaining the overall integrity of the film (Step 2). Subsequent UV irradiation reduces gold complex ions into Au^0 atoms while possibly oxidizing ammonium ions into imines, deprotonating them into amines, or allowing them to electrostatically bind to the carboxylates (Step 3).[50] The formation of Au^0 atoms facilitates nucleation and growth, with their relative rates determining the final density and size of the gold nanoparticles.[51,52]

(PAH9.3/PSS9.3) Multilayer System. Because of the high assembly pH, this multilayer film comprises a high concentration of free amine groups that are clustered in hydrophobic domains and, as a result, exhibit an unusually low pK_a (ca. 4).[36] In the low binding regime (pH >5.0), only a small fraction of the free amine groups in these hydrophobic domains are protonated and hence available to bind the gold complex ions; this situation results in the binding of a low concentration of gold complex ions. In the high binding regime (pH ≤5.0), the strong acidic condition protonates the amine groups into ammonium groups. The strong charge repulsion among the ammonium groups overcomes the hydrophobic interactions and the film undergoes a molecular rearrangement to produce a high concentration of free ammonium groups and a dramatic swelling transition (Scheme 1b, Step 1).[36,48] As a result, the gold salt binding capacity of the film increases dramatically, as indicated from the peak intensities and λ_{max} values of the SPR bands (Figure 1b).

Controlling Gold Nanoparticle Size and Spatial Distribution with Postassembly Processing Conditions. As discussed above, the significant increase in the gold salt loading capability and ultimately gold nanoparticle concentration for these two particular PAH-based multilayer systems is a direct consequence of molecular rearrangements that occur with low pH treatments. Given the quite different mechanisms underlying these molecular rearrangements, we set out to determine how this would influence the size and spatial distribution of the resultant gold nanoparticles.

(PAH7.5/PAA3.5) Multilayer System. We have previously found that multilayers of this type will undergo a transition to either a nanoporous or microporous state depending on the pH and salt concentration of the treatment solution.[1,3,49] The sensitivity of these molecular rearrangements to both parameters is demonstrated in two different postassembly processes leading to different types of porosity transitions, depending on the presence of gold complex ions. In particular, the multilayers were either (i) directly immersed in a gold salt solution at pH 1.8, which induces a nanoporosity transition to a higher extent than that at pH 2.3, or (ii) first immersed in acidic water (pH 2.5), which induces a microporosity transition in the multilayers before gold salt loading.

(i) Inducing Increased Nanoporosity with Gold Salt Loading at pH 1.8. As seen in Figure 1(a), a dramatic increase in the maximum intensity and λ_{max} value of the gold nanopar-

(50) Richardson, M. J.; Johnston, J. H.; Borrmann, T. *Eur. J. Inorg. Chem.* **2006**, 2618–2623.
(51) Mallick, K.; Witcomb, M. J.; Scurrell, M. S. *Appl. Phys. A: Mater. Sci. Process.* **2005**, *80*, 395–398.
(52) Kane, R. S.; Cohen, R. E.; Silbey, R. *Langmuir* **1999**, *15*, 39–43.

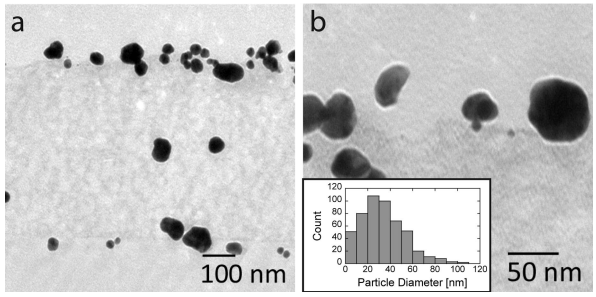

Figure 2. (a) Cross-sectional TEM image of a $(PAH7.5/PAA3.5)_{20}$ PEM (as-assembled dry film thickness 292 nm) loaded with pH 1.8 gold salt and UV-reduced. (b) TEM image at higher magnification. Inset: Particle size distribution. The average particle size is 33.4 ± 19.2 nm.

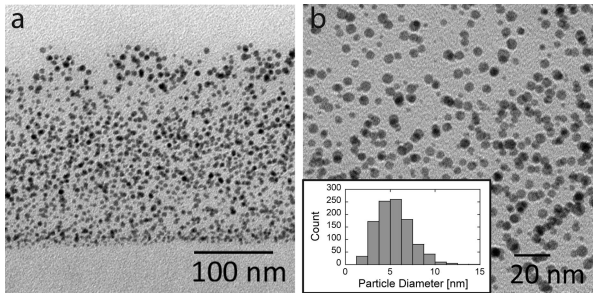

Figure 3. (a) Cross-sectional TEM image of a $(PAH7.5/PAA3.5)_{20}$ PEM (as-assembled dry film thickness 292 nm) loaded with pH 2.3 gold salt and UV-reduced. (b) TEM image at higher magnification. Inset: Particle size distribution. The average particle size is 5.5 ± 1.9 nm.

ticle SPR band occurs in this multilayer system when the gold salt loading pH changes from 2.3 to 1.8. Significant differences are observed in the cross-sectional TEM images of the films loaded at pH 1.8 (Figure 2) compared to those loaded at pH 2.3 (Figure 3), including (i) a much larger particle size with broader size distribution (33.4 ± 19.2 and 5.5 ± 1.9 nm, respectively), (ii) migration of nanoparticles toward the PEM surfaces, and (iii) a more apparent indication of development of a nanoporous structure. Migration of nanoparticles to multilayer surfaces and interfaces (Figure 2) has been reported in the literature, and is attributed to minimization of energy of the nanoparticles.[53] The formation of a nanoporous structure after the gold salt loading (pH 1.8) is confirmed by (i) an increase in the dry film thickness, (ii) a decrease in the dry film refractive index, and (iii) the transparent appearance of the film (see the Supporting Information). These changes were observed after gold salt loading at pH 2.3 to a much lesser extent. It therefore appears that with the presence of gold complex ions, the nanoporosity transition is partially triggered at pH 2.3 and proceeds to a much higher extent at pH 1.8. It had been reported that without gold complex ions, a microporosity transition occurs at pH 2.5, which is apparent from the translucent appearance of the film.[1,3,49] In our case, the multilayers remain transparent after immersion in gold salt solution at pH 2.3, which indicates that a transition to the nanoporous state as opposed to a microporous state is facilitated by the presence of the gold complex ions. These observations are consistent with previous findings, which demonstrated the sensitivity of the length scale of the porosity transitions to both pH and salt concentration of the treatment solutions.[1,3,49] For instance, immersing the films in acidic water at pH 1.8 and 2.5 triggers porosity transitions in the nanometer and micron scales, respectively, indicated from the transparent and translucent appearances (respectively) of the films. With the presence of salt (pH 2.4, 0.05 M $MgCl_2$), however, the film appeared transparent, and it was found that the porosity transition length scale had shifted to the nanometer range.

Polymers containing amine groups function as gold nanoparticle stabilizing and capping agents in solution-based gold nanoparticle syntheses.[35,54] In general, a high amine-to-gold complex ion ratio leads to the formation of gold nanoparticles of smaller sizes because of the effective stabilization of the gold nanoparticles by the amine groups. On the other hand, at a low amine-to-gold complex ion ratio, the nanoparticles formed are larger and tend to aggregate because of an inadequate number of amine groups stabilizing the gold nanoparticles. In our case, the dramatic molecular rearrangements that occur during the porosity transition at pH 1.8 (with the presence of gold complex ions) lead to the binding of a high concentration of gold complex ions to the free ammonium groups that are spatially sparser, resulting in gold nanoparticles that are less effectively stabilized and hence the significant increase in particle size (ca. 33 nm, up to 100 nm) and the aggregation of nanoparticles compared to those loaded at pH 2.3. Comparisons of the UV−vis absorbance spectra of the films immersed in gold salt solutions at pH 1.8, 2.3, and 5.2 without UV reduction (see the Supporting Information) confirm the significant increase in the concentration of gold complex ions bound to the films at lower pH levels. The porosity transition during gold salt loading (pH 1.8) is confirmed by a 2-fold dry film thickness increase from 290 to 580 nm. When exposed to UV light, the previously expanded multilayer structure collapses as indicated by the dry film thickness decrease from 580 to 360 nm. Control experiments eliminated the possibility of convective heating from the UV lamp and demonstrated that the dry film thickness decrease is only observed for films that had been previously immersed in solutions containing gold salt. The densification of the multilayer film can be attributed to the electrostatic binding of carboxylates to ammonium groups that were previously bound to the gold complex ions; reduction of gold complex ions into Au^0 atoms upon UV irradiation renders the ammonium groups free for binding.

Utilizing the changes in the dry film thickness with gold salt loading and reduction, we demonstrate a method of constructing 3-D patterns on PEMs by immersing the films into a gold salt solution (pH 1.8, 15 min) and subsequently exposing the film to UV light through a photomask (20 μm holes, 50 μm apart). The plan view of stacked confocal microscopy images (Figure 4) shows circular patterns which represent the UV-reduced region; the remaining portions of the film are regions loaded with unreduced gold complex ions. From the plan view image, the latter regions indicate a mostly porous structure (consistent with the decrease in

(53) Joly, S.; Kane, R.; Radzilowski, L.; Wang, T.; Wu, A.; Cohen, R. E.; Thomas, E. L.; Rubner, M. F. *Langmuir* **2000**, *16*, 1354–1359.

(54) Kuo, P. L.; Chen, C. C.; Jao, M. W. *J. Phys. Chem. B* **2005**, *109*, 9445–9450.

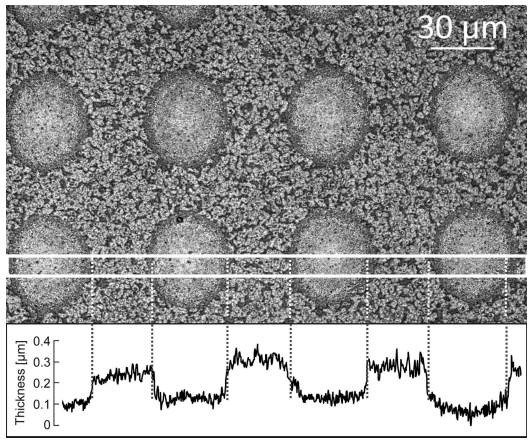

Figure 4. Confocal microscopy plan view image of a $(PAH7.5/PAA3.5)_{20}$ PEM loaded with pH 1.8 gold salt and UV-irradiated through a photomask (20 μm diameter holes, 50 μm apart). Below: Thickness profile averaged over 10 μm (rectangular box height).

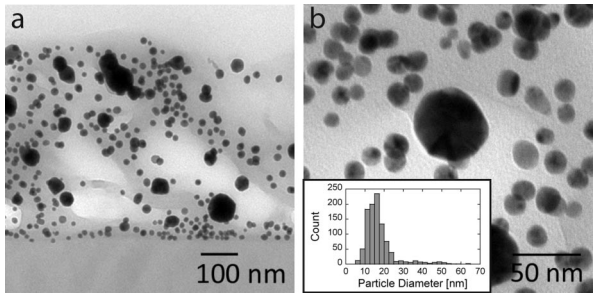

Figure 5. Cross-sectional TEM image of a $(PAH7.5/PAA3.5)_{20}$ PEM immersed in acidic water (pH 2.5) prior to gold salt loading (pH 2.3) and UV reduction. Inset: Particle size distribution. The average particle size is 17.3 ± 9.0 nm.

the refractive index) which appears to densify in regions exposed to UV light. The average diameter and depth of the cylindrical holes are 40 μm and 183 nm, respectively. The larger feature size on the sample compared to that of the photomask is most likely due to nonunidirectional UV irradiation past the photomask.

(ii) Inducing Microporosity in the Multilayers Prior to Gold Salt Loading. As mentioned above, at a gold salt loading pH of 1.8, the nanoporosity transition generates free ammonium groups that are spatially sparse, thereby resulting in larger gold nanoparticles that tend to aggregate. As an alternative approach to controlling the spatial density of the ammonium groups, we first immersed the films in acidic water (pH 2.5), which triggers a microporosity transition in the multilayers.[1,3,49] The microporous structure of the film was confirmed from the 2-fold thickness increase (from 293 to 575 nm) and the translucent appearance of the film due to light scattering from the pores. We then examined gold salt loading in the microporous films at three pH levels: 1.8, 2.3, and 5.2. We observed very similar trends in the UV−vis absorbance spectra (see the Supporting Information) compared to those of the as-prepared multilayers. In particular, both the SPR intensity and λ_{max} values increase with decreasing loading pH, with a significant increase at pH 1.8. It thus appears that similar to the as-prepared films, successful gold salt loading in the preformed microporous films requires the breaking of the electrostatic bonds between the carboxylates and ammonium groups at a low pH. We also observed

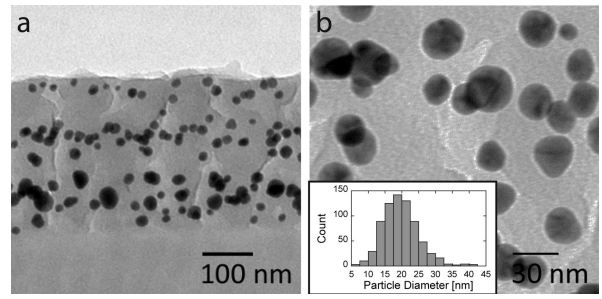

Figure 6. (a) Cross-sectional TEM images of $(PAH9.3/PSS9.3)_{20}$ PEMs immersed in gold salt at pH 2.3 and UV reduced. (b) TEM image at higher magnification. Inset: Particle size distribution. The average particle size is 20.3 ± 5.6 nm.

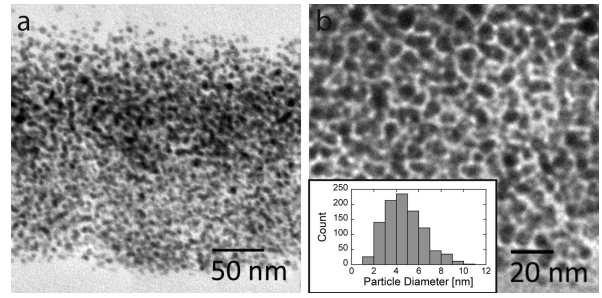

Figure 7. (a) Cross-sectional TEM images of $(PAH9.3/PSS9.3)_{20}$ PEMs immersed in gold salt at pH 5.2 and UV reduced. (b) TEM image at higher magnification. Inset: Particle size distribution. The average particle size is 4.7 ± 1.7 nm.

from the cross-sectional TEM images that the gold nanoparticles formed in the microporous films at a loading pH of 2.3 are larger ($\mu = 17.3 \pm 9.0$ nm, Figure 5) than those formed in the as-prepared films at this same pH ($\mu = 5.5 \pm 1.9$ nm, Figure 3), which is attributed to the lower spatial density of ammonium groups in the microporous film. The lighter regions in the TEM image (Figure 5) are indicative of the microporous structure in the film.

(PAH9.3/PSS9.3) Multilayer System. As discussed above, in this multilayer system, molecular rearrangements triggered by low pH treatments lead to a swelling transition and a substantial increase in gold salt loading capability. We now explore how this transition influences the resulting gold nanoparticle size and spatial distribution by comparing the results obtained when the swelling transition is triggered with or without the presence of gold complex ions.

(i) Inducing the Swelling Transition with Gold Salt Loading. In this case, the multilayer films were directly loaded with gold salt at pH levels above and below the critical loading pH for this system and then exposed to UV light. Cross-sectional TEM images of the resulting multilayer films show that the gold nanoparticles formed at a loading pH of 2.3 ($\mu = 20.3 \pm 5.6$ nm, Figure 6) are much larger than those formed at pH 5.2 ($\mu = 4.7 \pm 1.7$ nm, Figure 7), because of the dramatic increase in the concentration of gold complex ions bound to the film during the low pH-triggered swelling transition, which is confirmed by the UV−vis absorbance spectra of the films loaded with gold salt solutions at different pH levels without UV reduction (see the Supporting Information). The increase in nanoparticle size also correlates with the extent of swelling of the film which increases from 42 to 99% as the loading pH changes from

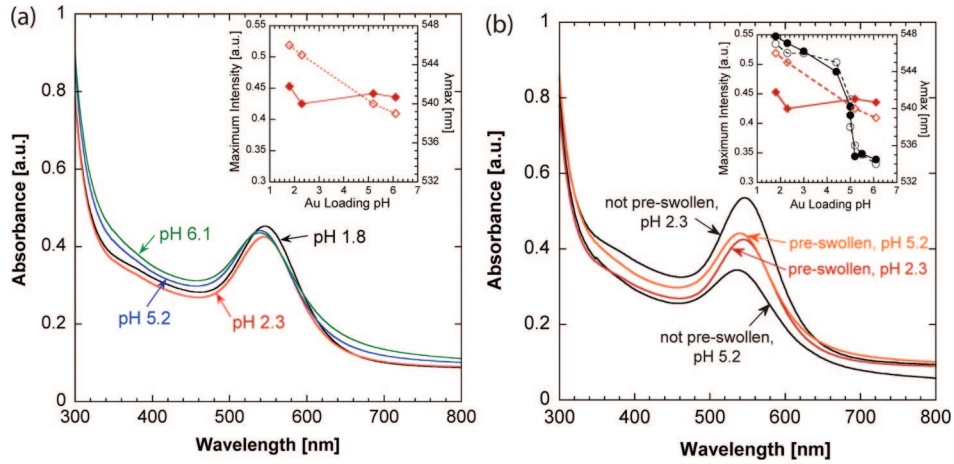

Figure 8. (a) UV−vis absorbance spectra of preswollen $(PAH9.3/PSS9.3)_{20}$ PEMs treated with acidic water (pH 2.5), immersed in gold salt solutions at different pH levels and UV reduced. Inset: SPR maximum intensity (closed diamonds) and λ_{max} (open diamonds) from the SPR absorbance spectra as a function of gold loading pH. (b) UV−vis absorbance spectra of both preswollen and not-pre-swollen $(PAH9.3/PSS9.3)_{20}$ PEMs immersed in gold salt solutions at different pH levels and UV reduced. Inset: SPR maximum intensity (closed) and λ_{max} (open) from the SPR absorbance spectra as a function of gold loading pH. Red, preswollen; black, not preswollen.

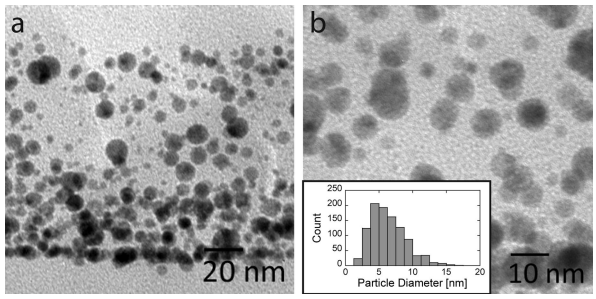

Figure 9. (a) Cross-sectional TEM image of a $(PAH9.3/PSS9.3)_{20}$ PEM immersed in acidic water (pH 2.5) followed by gold solution (pH 5.2) and then UV-reduced. (b) TEM image at higher magnification. Inset: Particle size distribution. The average particle size is 6.4 ± 2.8 nm.

5.2 to 2.3 (see the Supporting Information). It is worth noting that these extents of swelling are still much lower than that of a film immersed in acidic water (pH 2.5) without gold complex ions (611%). As in the case of the microporosity transition in the (PAH7.5/PAA3.5) multilayer system, we find that the presence of gold complex ions influences the process. Further work is needed to understand how the swelling transition is influenced by the presence of gold complex ions in the (PAH9.3/PSS9.3) multilayer system, although it is likely that electrostatic shielding effects are playing an important role.

(ii) Inducing the Swelling Transition Prior to Gold Salt Loading. We demonstrate here a method of generating gold nanoparticles of a different size and spatial distribution, which involves first inducing the swelling transition by acidic water (pH 2.5) without the presence of gold complex ions prior to gold salt loading. Previous work on this multilayer system showed that after an acidic water treatment, the film retains its swollen state even when immersed in solutions of higher pH, up to ca. 10.5.[48] The preservation of the extent of swelling of the films after immersion in acidic water and subsequently the gold salt solution was confirmed by the similarity of the film thicknesses in both solutions (see the Supporting Information). We therefore expected the concentrations of gold complex ions bound to the preswollen multilayers to be similar across loading pH 2−6, which was confirmed by UV−vis spectrophotometry (see the Supporting Information). As expected, the UV−vis absorbance spectra of the loaded and reduced multilayers (Figure 8a) show similar SPR intensities across the pH levels studied. The λ_{max} values, however, increase with decreasing loading pH, thus suggesting an increase in the particle size at a lower loading pH. Comparisons of the UV−vis absorbance spectra of both preswollen and not-preswollen films (Figure 8b) reveal that the SPR maximum intensity and λ_{max} values of the preswollen films are slightly higher than those of the not-preswollen films in the low gold binding regime (pH >5.0), but lower in the high gold binding regime (pH ≤5.0). It therefore indicates that the preloading swelling transition (without gold complex ions) increases the gold binding capacity of the multilayers when loaded in the low gold binding regime, but decreases it in the high gold binding regime, which was confirmed by UV−vis spectrophotometry (see the Supporting Information). Consistent to the former trend, cross-sectional TEM images of multilayers loaded in the low gold binding regime (pH 5.2) show that the gold nanoparticles formed in the preswollen films (μ = 6.4 ± 2.8 nm, Figure 9) are somewhat larger than those formed in the not-preswollen films (μ = 4.7 ± 1.7 nm, Figure 7). We speculate that the decrease in the gold binding capacity of the preswollen multilayers arises from the binding of ammonium groups with Cl^- ions from the preloading acidic treatment; a dramatic decrease in the binding of gold complex ions by polymeric amine/ammonium groups due to saturation by Cl^- ions has been reported in literature.[50]

Design Rules for Systematic Control over the Size, Size Distribution, and Spatial Distribution of Gold Nanoparticles. We discuss in this section design parameters that allow systematic control over the size, size distribution, and spatial distribution of gold nanoparticles synthesized in situ in the two multilayer systems. Overall, the gold nanoparticles can exhibit two distinct sizes and spatial distributions depending on the postassembly processing conditions. In the first case, the nanoparticles are smaller with a relatively narrow size distribution, and are evenly distributed across

the film cross-sectional area. These characteristics are very similar to those observed in the carboxylic-acid−based in situ silver nanoparticle synthesis in the (PAH3.5/PAA3.5) multilayer system.[2,30,31] In this study, these characteristics were always observed in the (PAH9.3/PSS9.3) multilayer system within the gold salt loading pH levels studied (pH 1.8 to 6.1), but only observed in the (PAH7.5/PAA3.5) multilayer system at gold salt loading pH $\geq$2.3. In the second case, the nanoparticles have a significantly larger size with relatively broad size distribution, and tend to migrate to the multilayer surfaces. These characteristics can be generated in the (PAH7.5/PAA3.5) multilayer system through two processes: (i) by loading the multilayers in gold salt at pH 1.8, or (ii) by prefabricating a porous structure in the multilayers by an acidic water treatment (pH 2.5), followed by gold salt loading at pH $\leq$2.3. Thus it appears that the key factors dictating the gold nanoparticle size and spatial distribution are the concentration of gold complex ions bound to the film and the density of the amine/ammonium groups they reside on, which can be manipulated through the film assembly and postassembly processing conditions.

Conclusions

We demonstrate that successful in situ synthesis of gold nanoparticles in PEMs can be achieved provided the films, assembled at specific pH conditions, can generate free ammonium groups under suitable postassembly processing conditions. In particular, we show that in both (PAH7.5/PAA3.5) and (PAH9.3/PSS9.3) multilayer systems, the gold binding capacities of the films increase dramatically below pH values of about 2.5 and 5.0, respectively, compared to that at higher loading pH levels. These substantial differences in gold binding capacity arise from molecular rearrangements in the films that result in porosity and swelling transitions in the PEMs. The proposed gold binding mechanisms in both high and low gold salt binding regimes are supported by previous studies of postassembly molecular rearrangements in the same multilayer systems. Based on these gold binding mechanisms, the film assembly (e.g., pH) and postassembly processing conditions (e.g., gold salt loading pH and prefabrication of a porous structure prior to gold salt loading) can be manipulated for systematic control over the size and spatial distribution of the gold nanoparticles in the multilayers.

Acknowledgment. This work was supported by the MRSEC Program of the National Science Foundation under Grant DMR-02-13282. The authors thank the Center for Materials Science and Engineering (CMSE) and the Institute of Soldier Nanotechnologies (ISN) for the use of characterization equipments.

Supporting Information Available: UV−vis absorbance spectra of gold salt loaded and UV-reduced (PAH7.5/PAA3.5), (PAH3.5/PAA3.5), (PAH9.3/PSS9.3), and (PAH4.0/PSS4.0) PEMs. Dry film thicknesses of $(PAH7.5/PAA3.5)_{20}$ PEMs immersed in gold salt solutions at different pH levels, measured before and after UV irradiation. UV−vis absorbance spectra of $(PAH7.5/PAA3.5)_{20}$ PEMs immersed in gold salt solutions at different pH levels, measured before UV irradiation. UV−vis absorbance spectra of $(PAH7.5/PAA3.5)_{20}$ PEMs first immersed in acidic water, then in gold salt solutions at different pH levels and UV-reduced. UV−vis absorbance spectra of preswollen and not-preswollen $(PAH9.3/PSS9.3)_{20}$ PEMs immersed in gold salt solutions at different pH levels, measured before UV irradiation. Extent of swelling of $(PAH9.3/PSS9.3)_{20}$ PEMs in dry state, water, and gold salt solutions (PDF). This material is available free of charge via the Internet at http://pubs.acs.org.

CM802166S